MIT Open Access Articles

Sustainable Lithium Recovery from Hypersaline Salt-Lakes by Selective Electrodialysis: Transport and Thermodynamics

Massachusetts Institute of Technology

Sustainable Lithium Recovery from Hypersaline Salt-lakes by Selective Electrodialysis: Transport and Thermodynamics

Zi Hao Foo,[†,‡] John B. Thomas,[†] Samuel M. Heath,[†] Jason A. Garcia,[¶] and John H. Lienhard[*,†]

†Department of Mechanical Engineering, Massachusetts Institute of Technology,
Cambridge, Massachusetts 02139, United States

‡Center for Computational Science and Engineering, Massachusetts Institute of Technology,
Cambridge, Massachusetts 02139, United States

¶Department of Chemical Engineering, Massachusetts Institute of Technology,
Cambridge, Massachusetts 02139, United States

E-mail: lienhard@mit.edu

Abstract

Evaporative technology for lithium mining from salt-lakes exacerbates freshwater scarcity and wetland destruction, and suffers from protracted production cycles. Electrodialysis (ED) offers an environmentally benign alternative for continuous lithium extraction and is amendable to renewable energy usage. Salt-lake brines, however, are hypersaline multicomponent mixtures and the impact of the complex brine–membrane interactions remains poorly understood. Here, we quantify the influence of the solution composition, salinity and acidity on the counter-ion selectivity and thermodynamic efficiency of electrodialysis, leveraging 1250 original measurements with salt-lake brines that span four feed salinities, three pH levels and five current densities. Our experiments reveal that commonly used binary cation solutions, which neglect Na^+ and K^+ transport, may overestimate the Li^+/Mg^{2+} selectivity by 250 % and underpredict the specific energy consumption (SEC) by a factor of 54.8. As a result of the hypersaline conditions, exposure to salt-lake brine weakens the efficacy of Donnan exclusion, amplifying Mg^{2+} leakage. Higher current densities enhance the Donnan potential across the solution-membrane interface and ameliorate the selectivity degradation with hypersaline brines. However, a steep trade-off between counter-ion selectivity and thermodynamic efficiency governs ED's performance: a 6.25 times enhancement in Li^+/Mg^{2+} selectivity is accompanied by a 71.6 % increase in the SEC. Lastly, our analysis suggests that an industrial-scale ED module can meet existing salt-lake production capacities, while powered by a photovoltaic farm that utilizes <1 % of the salt-flat area.

Keywords: Selective Electrodialysis, Salt-lake, Lithium Recovery, Ion-exchange Membrane, Sustainable Mining

Synopsis

Electrodialysis selectively concentrates monovalent ions, facilitating direct lithium extraction from salt-lakes while eliminating the environmental impact of evaporation ponds.

1   Introduction

The demand for battery-grade lithium is expected to intensify by 40-fold, driven by the meteoric expansion of the electric vehicle market which will increase from several thousands vehicles in 2010 to over 142 million by 2030.[1–3] Over 89 million tons of lithium exists naturally in solid minerals (e.g., spodomene, laponite) and in continental and geothermal salt-lakes.[4,5] State-of-the-art evaporative technologies for salt-lake lithium harvesting, however, consume up to 800 m^3 of freshwater per ton of Li_2CO_3, aggravating water scarcity in some of the most arid regions of the world, while exacerbating aquifer pollution and wetland destruction from its reliance on evaporation ponds.[1,6–8] Lithium production is further bottlenecked by the protracted concentration cycles of evaporation ponds, which contribute to a price-inelastic supply that is unresponsive to market demand.[6,9,10]

To avoid the problems of evaporation ponds, lithium can instead be recovered with direct lithium extraction (DLE) technology. In DLE, ionic liquids,[12] eutectic solvents,[13–15] fractional crystallization,[16–18] electrochemical absorption[19,20] and chelating agents[21,22] are utilized either separately or synergistically to isolate lithium from a multicomponent mixture (e.g. Na^+, K^+). Further, by avoiding brine evaporation altogether, DLE can be viable for dilute lithium sources.[23] The high Mg^{2+} concentrations in salt-lake brines, however, attenuate the extraction effectiveness of DLE, as a result of the comparable solubility products and ionic radii of Li^+ and Mg^{2+}.[1,17,24] DLE methods to isolate Li from a Na-rich mixture typically requires the Li^+/Mg^{2+} ratio of the brine to be greater than 4 approximately to minimize chemical usage for precipitation and/or solvent recovery.[17,21] To enhance the selectivity and the atomic efficiency of DLE, the salt-lake brine can be pre-treated with membrane processes like nanofiltration (NF)[25–28] or electrodialysis (ED)[29–32] to eliminate multivalent cations. The prospect of ED for lithium concentration from salt-lakes is particularly promising because of its successful commercial history in salt production from hypersaline brines.[33,34]

In an electrodialysis module, cation- and anion-exchange membranes (CEM and AEM, respec-
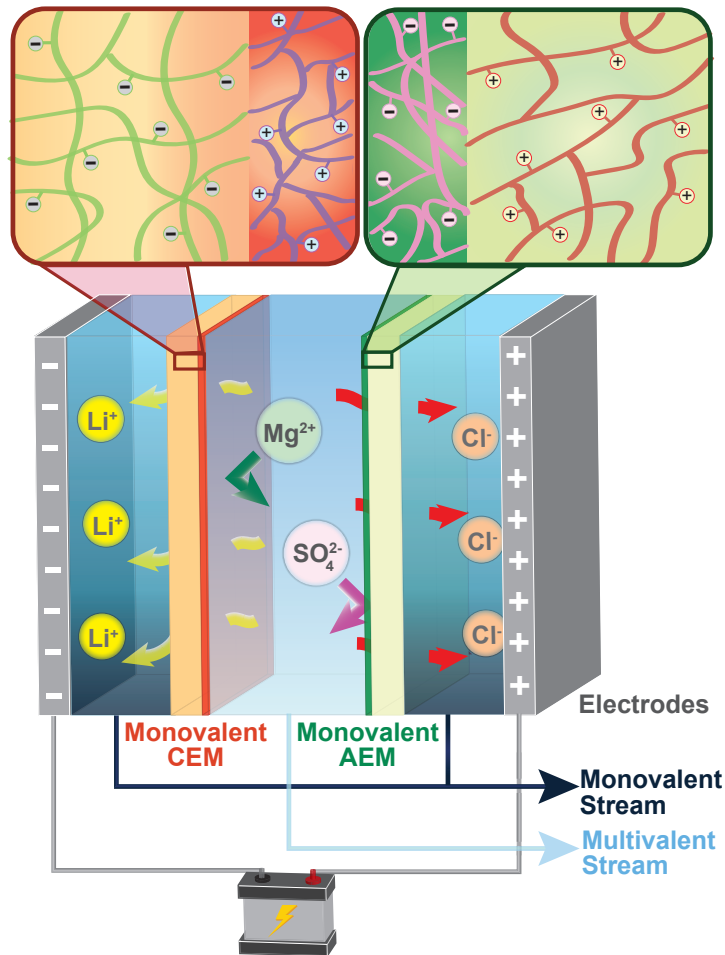
Figure 1: Schematic diagram of a cell pair in an electrodialysis unit with monovalent selective ion-exchange membranes. Industrial electrodialysis units typically comprise up to 100,000 repeating cell pairs.[11] Conventional cation- and anion-exchange membranes are negatively- and positively-charged water-swollen polymeric films with a typical thickness of 50 - 200 μm. To impart monovalent selectivity to the ion-exchange membranes, a highly-crosslinked positively- and negatively-charged surface coating is applied to the respective ion-exchange membrane to enhance counter-ion Donnan exclusion. In lithium concentration applications, a monovalent stream rich in Li$^+$ ions is recovered with selective electrodialysis.

tively) are arranged in an alternating order between two electrodes, separating the feed stream into diluate and concentrate product streams.[19,35] Conventional CEMs and AEMs are monopolar water-swollen polymeric films that typically contain negatively-charged perfluorosulfonic acid and positively-charged quarternary ammonium moieties, respectively.[36] As a result of the charged moieties, the electrostatic potentials that form along the solution-membrane interface inhibit ions of the same charge (i.e., co-ions) from partitioning into the interstitial phase of the membrane,[37–39] a phenomenon known as Donnan exclusion.[40,41] To impart monovalent cation selectivity,[42,43] typically a

thin polyethyleneimine (PEI) surface layer is covalently-bonded with the CEM substrate through a condensation reaction between the perfluorosulfonic acid and amine moieties.[31,36] As illustrated in Figure 1, the composite CEM acquires a positive zeta potential and exhibits passive selectivity for monovalent cations from the enhanced Donnan exclusion effect.[4,29]

Based on experiments with dilute binary cation solutions, selectivity enhancements in Li^+/Mg^{2+} separations with multi-layered or polyelectrolyte ion-exchange membranes are well documented in the literature.[4,31,32,43–45] As stressed in recent reviews on salt-lake lithium extraction, however, over 95 % of prior work disregard the deleterious impacts from competing ions, and the high feed salinity that is representative of salt-lake brines.[1,4,19] Our experiments reveal that, when binary cation solutions are utilized in place of salt-lake brines, the apparent Li^+/Mg^{2+} selectivity may be overestimated by a factor of 2.5 and that the specific energy consumption may be underpredicted by a factor of 54.8. In lithium extraction applications, the feed solution is typically acid pre-treated to a pH of 3 or lower, to mitigate carbonate and phosphate scaling risks;[5,19,46] majority of the charged moieties in commercial IEMs are based on weak organic acids, and the repercussions of the acidic conditions on the IEM's selectivity remains unanswered.[36,47] Further, in hypersaline conditions, the performance of electrodialysis is bounded by a steep trade-off between counter-ion selectivity and thermodynamic efficiency which appears to be governed by the current density. A formal mathematical treatment of the complex current density phenomena, however, remains elusive.

Here, we quantify the kinetics of ion transport across composite ion exchange membranes, and unravel the inherent dependence of the thermodynamic efficiency and ion selectivity on intrinsic membrane properties, applied current density and the solution composition, salinity and acidity. Our conclusions are derived based on 1250 original concentration measurements that span four feed salinities, three pH levels and five current densities, using brines that model two industrial salt-lakes. The measurements are used to calibrate a multi-ionic transport model to derive mechanistic insights on the thermodynamics of ion selectivity and are systematically compiled in the Supporting Information (SI). By juxtaposing the binary cation and salt-lake solution experiments, we deconvolute the coupled ion transport kinetics, revealing the influence of Na^+ and K^+ competition and solution concentration on the apparent ion selectivities and energy efficiencies. Finally, we assess the implications on the process duration and land area requirements, for salt-lake lithium concentration with electrodialysis.

2 Materials and Methods

2.1 Chemicals and Materials

Composite monovalent selective ion exchange membranes (Neosepta CMS & ACS) were obtained from Astom Corporation (Tokyo, Japan).[35] According to open literature, the cation exchange membrane (CEM) is composed of a polystyrene-divinyl benzene (PS-DVB) substrate with negatively charged perfluorosulfonic acid moieties and a polyethyleneimine (PEI) surface layer with positively charged quaternary ammonium moieties.[36,37]

Experiments are conducted with synthetic salt-lake brines from Salar de Atacama, Chile and Qaidam Lake, China (Table 1).[44,48] Anhydrous NaCl, KCl, LiCl, $MgCl_2$, Na_2SO_4, K_2SO_4, Li_2SO_4, $MgSO_4$, NaOH (> 98 %) and HCl (37 %) are procured from MilliporeSigma. Type 1 ultrapure water (18.2 MΩ cm) is used to prepare all stock solutions. To investigate the effects of feed salinity, the respective salt-lake brines are diluted while keeping the relative ionic ratios constant (Table S3 and S4 in SI). Experiments at solution pH of 7, 5 and 3 are conducted to investigate the impact on ion partitioning and the specific energy consumption. Complementary experiments are conducted with binary cation feed solutions comprising Li^+ and Mg^{2+} cations to ascertain multicomponent solution effects (Table S2 in SI).[28]

2.2 Experimental Characterization

Over 1250 original ion concentration measurements are collected using binary cation solutions and multicomponent salt-lake brines, and are systematically tabulated in the Supp. Tables 5–39. A full description of the apparatus and the rationale of the experimental design appears in the SI (Section B.1 in SI). A bench scale electrodialysis system (PCCell ED 200) is configured to characterize the performance of the ion exchange membranes (IEM), comprising 10 repeating cell pairs with a total membrane area of 0.43 m^2. The experiments are conducted at a temperature of 20 °C and at atmospheric pressure. The total dissolved solid (TDS) concentration of the feed solution ranges from 10 to 250 g L^{-1}, at a solution pH of 3, 5 and 7, to simulate the effects of the high feed salinity and acid pre-treatment in salt-lake applications.[5,24] Ion selectivity of the IEMs is evaluated with constant current experiments, using current densities ranging between 2.5 to 30.0 mA cm^{-2}. The

Table 1: Nominal ionic composition of the hypersaline brine from salt-lake reservoirs in Chile and China.

Salt Lake, Location	Nominal Composition (g L^{-1})						
	Li$^+$	Na$^+$	K$^+$	Mg^{2+}	Cl$^-$	SO$_4^{2-}$	TDS
Salar de Atacama, Chile[48]	1.19	69.01	17.89	7.31	143.72	12.06	251.18
Qaidam Lake, China[44]	0.31	56.30	4.40	20.20	134.20	34.10	249.51

solution pH is adjusted with dropwise addition of NaOH (1 M) and HCl (1 M).

For surface activation, the IEMs are first immersed in HCl (1 M) for 4 hours and then stored in ultrapure water for at least 24 hours.[49] Subsequently, to ensure membrane stability for ion selectivity, the membranes are equilibrated with the electrolyte streams in the ED cell for at least 4 hours before any potential difference is applied.[32,50] Experiments are conducted in increasing order of feed concentrations to mitigate the influence of structural changes on selectivity.[49] Aqueous samples from the diluate and concentrate loops are collected in centrifuge tubes periodically and chilled. The ionic composition of the samples are determined with inductively coupled plasma optical emission spectroscopy (Agilent ICP-OES 5100), using a five-point calibration curve based on standards from MilliporeSigma (Trace-Cert). Based on triplicate sampling, the maximum uncertainty in each concentration measurement is under 4.5 %. Tangential streaming potential measurements are collected on pristine and aged IEMs in a 100 μm gap cell (Anton Parr SurPASS 3) between the solution pH of 2 to 8.[51] The IEMs are aged by soaking in a 250 g L^{-1} Chilean brine solution for at least 7 days before streaming potential analysis to simulate operation with salt-lake brines, in accordance with Ying et al.'s method.[49] The zeta potential is subsequently calculated with the classical Smoluchowski equation.[52]

2.3 Computational Analysis

A multi-ionic transport model based on the Nernst-Planck equation is developed to quantify the selectivity and transport enhancements.[11,53,54] A full derivation of the transport equations appears in the SI (Section A.1 in SI). Across each computational node, as illustrated in Figure 2A, the molar ion and water fluxes are calculated with Eq. 1 and 2, respectively

$$J_i(x) = \left\{ \frac{\tau_i I_{den}}{z_i F} + B_i \left[C_i^{d,int}(x) - C_i^{c,int}(x) \right] \right\} \tag{1}$$
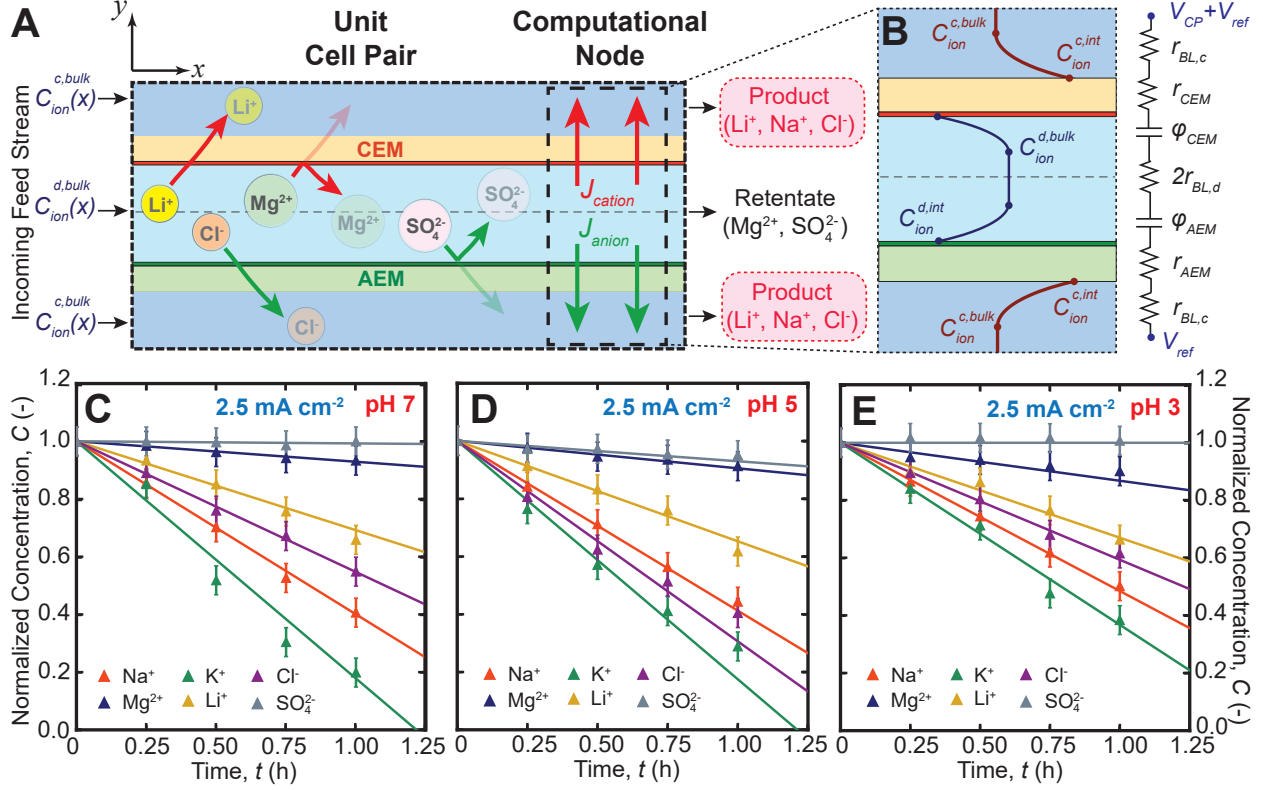
7

Figure 2: Schematic diagram illustrating the transport model for selective electrodialysis: (**A**) Computational node depicting one cell pair, comprising the diluate and concentrate streams, and the ion exchange membranes. Ionic flux is calculated while ensuring that the electrolyte streams remain electroneutral; (**B**) Decomposition of one cell pair into ohmic resistances and Donnan potentials, and a pictorial depiction of concentration boundary layers within the electrolyte streams; Comparisons between the experimental measurements (solid markers) and model predictions (solid lines) for multicomponent brines from Salar de Atacama, Chile, under a constant current density of 2.5 mA cm^{-2} at pH (**C**) 7, (**D**) 5 and (**E**) 3, respectively.

$$J_w(x) = \left\{ \frac{\tau_w I_{den}}{F} + A_w \left[\pi^{c,int}(x) - \pi^{d,int}(x) \right] \right\} \frac{M_w}{\rho_{mix}(x)} \tag{2}$$

where J_i (mol m^{-2} s^{-1}) and J_w (mol m^{-2} s^{-1}) denote the molar ion and water fluxes, τ_i (-) and τ_w (-) denote the ion and water transport numbers, I_{den} (A m^{-2}) denotes the applied current density, A_w (s m^{-1}) and B_i (m s^{-1}) denote the water and ion permeability coefficient for diffusion, $\pi^{c,int}$ (Pa) and $\pi^{d,int}$ (Pa) denote the osmotic pressure along the fluid-membrane interface in the concentrate and diluate streams, $C^{c,int}$ (mol m^{-3}) and $C^{d,int}$ (mol m^{-3}) denote the concentration of ion i in the concentrate and diluate streams along the same interface, and z_i (-), F (C mol^{-1}), M_w (g mol^{-1}) and ρ_{mix} (kg m^{-3}) denote the ionic valency, Faraday's constant, molar mass and mixture density, respectively.

8

The model incorporates ion and water transport from electromigration and diffusion. The ion transport rate by electromigration is governed by the transport numbers; the transport number is defined as the proportion of current conducted by the ion relative to the total applied current, characterizing the combined effects of ion partitioning and mobility across the IEM.[55,56] The ion and water permeability coefficients are analogous to the conventional parameters used in diffusion models,[57] and are regressed from multi-ionic diffusion experiments as reported in our prior publications.[35,53,58] Concentration polarization effects in the electrolyte streams, as depicted in Figure 2B, are incorporated based on mass transfer correlations for the spacers adopted in our experiments[11] (Eq. 11 in SI). The diffusion coefficients, density and viscosity of the multi-ionic solutions are calculated from empirical correlations.[59–61] The limiting current density of the each ion is calculated to ensure that the experiments are conducted within the ohmic regime (Eq. 13 in SI).[62] Across the solution-membrane interface, the Gibbs free energy of the ions is assumed to be continuous to ensure chemical stability. The ratio of the ion activity within the membrane polymer relative to the solution along the interface can be expressed as Eq. 3[39]

$$\frac{\gamma_i^{mem} C_i^{mem}}{\gamma_i^{d,int} C_i^{d,int}} = f_w \left[\exp\left(-\frac{z_i F}{RT} \Delta\phi_{Donnan} \right) \right] \tag{3}$$

where f_w (-) represent the water volume fraction within the membrane, $\Delta\phi_{Donnan} = \phi_i^{mem} - \phi_i^{d,int}$ (V) denote the Donnan potential and, γ_i^{mem} (-) and $\gamma_i^{d,int}$ (-) represent the ion activity coefficient within the membrane polymer and in the solution along the membrane-solution interface, respectively. The activity coefficients γ_i^{mem} and $\gamma_i^{d,int}$ are estimated with Manning's counter-ion condensation[63–65] and Pitzer-Kim models.[66,67] Eq. 3 is solved with electroneutrality conditions within the solution and the IEM (Section A.2 in SI) to determine the partitioned ion concentrations (C_i^{mem}).[68]

The apparent ion diffusion coefficient within the polymer matrix decreases from spatial hindrance from the tortuosity of interstitial phase,[56] and the electrostatic friction between the ions and the ion exchange groups.[69] The ion diffusion coefficient within the interstitial phase of the IEM can be calculated with the extended Mackie-Meares framework,[56] as provided in Eq. 4

$$D_i^{mem} = D_i^{d,int} \left(\frac{f_w}{2 - f_w} \right)^2 \exp(-A_{el} z_i^2) \tag{4}$$

9

where D_i^{mem} (m^2 s^{-1}) and $D_i^{d,int}$ (m^2 s^{-1}) denote the ion diffusion coefficient within the membrane and solution phases, respectively, and A_{el} (-) represents an electrostatic friction parameter that is a function of the fixed charge density (C_{fixed}^{mem}) and the apparent dielectric constant.[56] The Nernst-Planck, Donnan equilibrium and Mackie-Meares equations can be condensed to obtain an explicit expression for the ionic flux ratio, as described by Eq. 5 (see Section A.2 in SI)

$$\frac{J_i}{J_j} = \frac{D_i^{d,int}}{D_j^{d,int}} \frac{z_i}{z_j} \frac{C_i^{d,int}}{C_j^{d,int}} \overline{\gamma}_{i,j} \exp\left[-A_{el}\left(z_i^2 - z_j^2\right)\right] \exp\left[-\frac{\Delta\phi_{Donnan}F}{RT}\left(z_i - z_j\right)\right] \tag{5}$$

where $\overline{\gamma}_{i,j}$ (-) represents the ratio of activity coefficients between the solution and the interstitial phase, between species i and j, respectively. In this expression, the Donnan potential and the interfacial concentrations are functions of the applied current density.

In this study, a two-pronged computational approach is adopted to investigate the ion selectivity of the composite cation exchange membranes (Section A.3 in SI). The governing conservation equations for species and charge are discretized and solved in Python. The water and ion permeability coefficients are obtained from diffusion experiments in our prior publication.[35] The ion transport numbers, Donnan potential and the electrostatic friction parameter, at each solution pH, salinity and current density, are regressed from the experimental measurements using a constrained trust region method as described in Eq. 6, with a convergence criteria of 10^{-8} for the L^2-norm error[70]

$$\boldsymbol{\tau}_{opt}, A_{el,opt}, \Delta\phi_{opt} = \underset{\boldsymbol{\tau}, \boldsymbol{A_{el}}, \boldsymbol{\Delta\phi}}{\operatorname{argmin}} \left\{ \frac{||\boldsymbol{J}^{model}(\boldsymbol{\tau}, A_{el}, \Delta\phi) - \boldsymbol{J}^{exp}||_2}{N} \right\} \tag{6}$$

where $\boldsymbol{J}, \boldsymbol{\tau} \in \Re^N$, $A_{el}, \Delta\phi \in \Re^1$, $\boldsymbol{J}^{exp}$ (mol m^{-2} s^{-1}) and $\boldsymbol{J}^{model}$ (mol m^{-2} s^{-1}) denote the molar flux vectors from the experiments and model, respectively.

2.4 Performance Metrics

To ascertain the current carrying capacity of an ion across the CEM, the current utilization for Li$^+$ and the monovalent cations are calculated with Eq. 7 and 8, respectively[34]

$$\xi_{Li} = \frac{z_{Li} J_{Li}}{\sum_j^N z_j J_j} \tag{7}$$

$$\xi_{Mono} = \frac{z_{\mathrm{Li}} J_{\mathrm{Li}} + z_{\mathrm{Na}} J_{\mathrm{Na}} + z_{\mathrm{K}} J_{\mathrm{K}}}{\sum_{j}^{N} z_{j} J_{j}} \tag{8}$$

where ξ_{Li} (-) and ξ_{Mono} (-) represent the current utilization for Li^{+} and the monovalent cations. The ion selectivity between species i and j of the IEM is defined as the ratio of the ion fluxes normalized by their initial concentrations, as described by Eq. 9[71]

$$\alpha_{i/j} = \frac{J_i/J_j}{C_i^{d,bulk}/C_j^{d,bulk}} \tag{9}$$

where $\alpha_{i/j}$ (-) denote the separation factor between species i and j. To ensure valid comparison between experiments, the expected value and the uncertainty of the separation factors were calculated with our validated model, considering the region where a strong linear relationship between the transient concentration and time exists.

The specific energy consumption ($\mathrm{SEC}_{\mathrm{Li}}$), defined as the amount of electrical work consumed per mole of Li recovered, is computed with the time-varying cell voltage (V_{cell}) and the diluate stream volume ($\underline{V}^d(t)$), as described in Eq. 10[72]

$$\mathrm{SEC}_{\mathrm{Li}}(t) = \frac{I_{den} A_{mem} \int_0^t V_{cell}(t')\mathrm{d}t'}{C_{\mathrm{Li}}(0)\underline{V}^d(0) - C_{\mathrm{Li}}(t)\underline{V}^d(t)} \tag{10}$$

Lastly, the thermodynamic (Second Law, η^{II}) efficiency, denoting the process efficiency relative to the thermodynamic reversible limit, is calculated with Eq. 11[73]

$$\eta^{II}(t) = \frac{\bar{G}(t) - \bar{G}(0)}{I_{den} A_{mem} \int_0^t V_{cell}(t')\mathrm{d}t'} \tag{11}$$

where $\bar{G}(t)$ (J) denotes the Gibbs free energy of the solutions at time t (s), calculated using the Pitzer-Kim model.[66,67]

3   Results and Discussion

3.1   Computational Predictions Align with Empirical Measurements

The transient behaviors of the normalized ion concentrations for Chilean and Chinese salt-lake brines are summarized in Figure 2C-E and in Supp. Figure 2-11, for TDS concentrations ranging between

10 to 250 g L^{-1}, solution pH ranging between 3 to 7, and current densities ranging between 2.5 to 30.0 mA cm^{-2}. Strong agreement between the model predictions and empirical measurements is obtained, registering absolute deviations of 15 % or lower across all tested compositions. Under an applied current density of 2.5 mA cm^{-2} or greater, the transient ion concentrations exhibit a strong linear correlation with the process duration ($\min_i r_i^2 \approx 0.97$) in all of our experiments, ensuring valid comparisons in the respective separation factors. Further, this suggests that ion transport by electromigration is dominant, which is in agreement with the literature.[74,75] In descending order of cation selectivity, the relative slopes of the transient ion concentrations follow the sequence: $K^+ > Na^+ > Li^+ > Mg^{2+}$, which aligns with the recent empirical evidence for cation partitioning.[76,77]

At a solution pH of 7, under a feed salinity of 10, 30 and 70 g L^{-1}, the recorded current utilization for monovalent cation transport is 97.7, 96.6 and 91.1 %, respectively, which are within 10 % of empirical measurements with PEI-based CEMs.[35,49] The Na^+/Mg^{2+} and K^+/Mg^{2+} separation factors are 3.31 and 3.14 with a 10 g L^{-1} feed solution, and 2.23 and 2.30 with a 30 g L^{-1} feed solution, each falling within the respective uncertainty bounds from recent publications.[78] The measured zeta potentials of the PEI layer of the CEM lie within the standard errors from prior streaming potential experiments.[49]

The ion-exchange membranes are chemically stable for the solution pH between 0 to 8,[58] and all of our experiments were conducted within the stipulated pH range. Further, as observed from strong linear relationship of the concentration-time plots, it appears that the small pH change did not have a major influence on the trend in the relative ion transport rates.

3.2 Monovalent Selectivity from Donnan Exclusion Degrades with High Feed Concentration and Acidity

While copious reports on selectivity enhancements by Donnan exclusion are available in the literature, the conclusions are derived from experiments with binary cation (Li^+, Mg^{2+}) solutions that are both neutral and dilute, conditions that may not generalize for salt-lake applications.[4,45] As stressed in a recent review on salt-lake lithium extraction, fewer than 5 % of the membrane literature considered the impact of competing cations and the high feed salinities that are representative of salt-lakes.[1] Further, to the best of the authors' knowledge, the influence of the strong acidity of
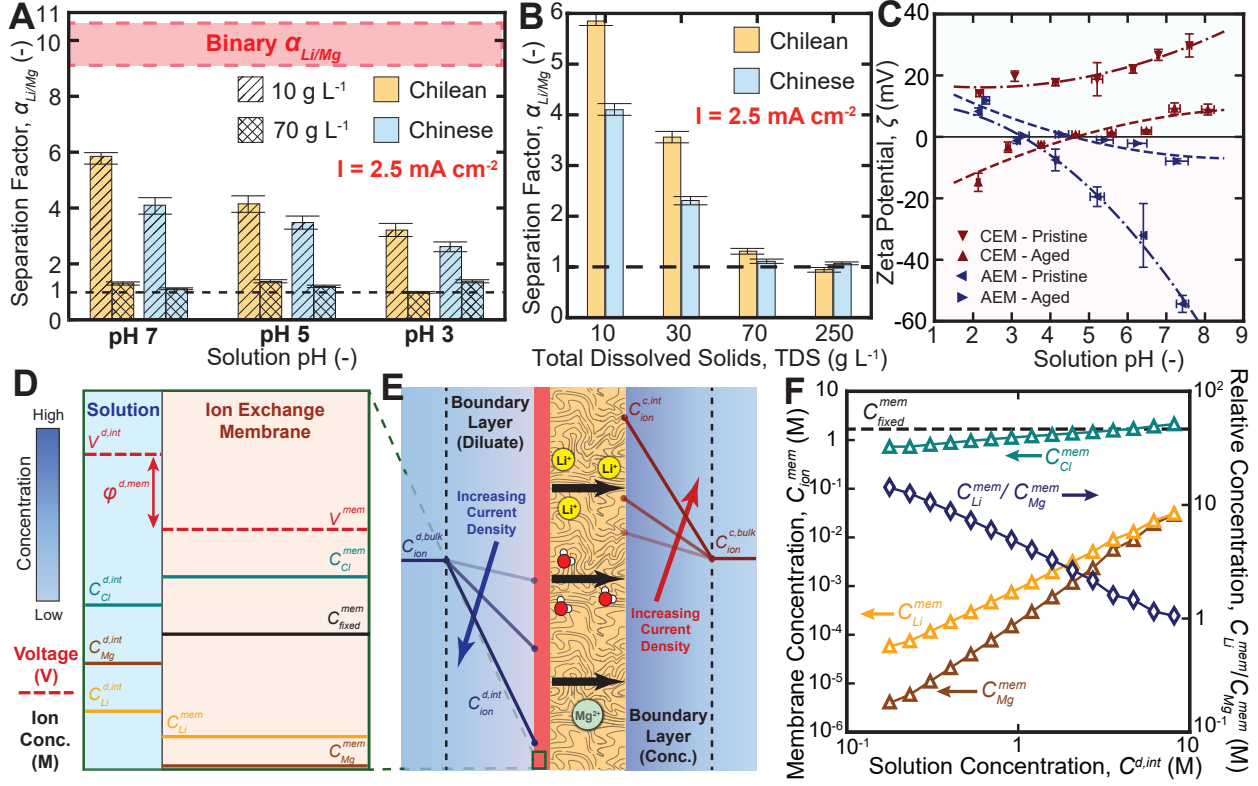
Figure 3: Plot of the Li^+/Mg^{2+} separation factor for binary cation solutions and Chilean and Chinese salt-lake brines as a function of (**A**) solution pH and (**B**) feed concentration, driven by a current density of 2.5 mA cm^{-2}. Binary cation solutions overestimate the Li^+/Mg^{2+} separation factors by up to three times because the competing effects from Na^+ and K^+ ions are neglected. Between the experiments with salt-lake compositions, the Li^+/Mg^{2+} separation factors decay with increasing feed concentrations and acidity; (**C**) Plot of the interfacial zeta potential as a function of solution pH and composition, for pristine CEMs and CEMs aged by hypersaline brines. The solid curves are polynomial interpolations intended for visualization only. The inclusion of the PEI surface layer yielded positive zeta potential for the CEM. The apparent zeta potential of the CEM fell by 24.7 mV on average after ageing in 250 g L^{-1} Chilean brines; (**D**) Nomenclature of the respective parameters along the solution-membrane interface; (**E**) Schematic diagram illustrating the depletion and concentration zones within the boundary layers of the diluate and concentrate electrolyte streams. The boundary layer phenomenon is more pronounced under higher current densities, arising from the greater mobility of ions than water within the ion exchange membranes;[81] (**F**) Concentration of Li^+, Mg^{2+} and Cl^- ions within the PEI layer of the CEM for a constant volumetric charge density, as a function of the external solution concentration along the fluid-membrane interface. Relative concentrations of Li^+ to Mg^{2+} decay with increasing solution concentration, arising from weakening Donnan exclusion effects.[39]

post-treated brines on the IEM's selectivity is nuanced and has yet to be fully explained.[79,80] To address these knowledge gaps, we conduct experiments with multicomponent acid-treated brine and quantify their impacts on the ion selectivity with our computational frameworks.

Figures 3A and B illustrate the Li^+/Mg^{2+} separation factors of the composite CEM as a func-

13

tion of the solution pH and feed salinity, under a current density of 2.5 mA cm^{-2}. The separation factors are evaluated based on experiments with Chilean[48] and Chinese[44] salt-lake brines, and with binary cation solutions that are commonly adopted in the literature.[8,28,31,44,82] Our results indicate that PEI-composite CEMs are monovalent selective, registering Li$^+$/Mg^{2+} separation factors greater than unity for the salt-lake solutions. However, our experiments reveal that Li$^+$/Mg^{2+} separation factors are overestimated by 50 to 250 % with binary cation solutions of the same molarity and Li$^+$/Mg^{2+} ratio; based on recent empirical evidence on ionic competition for intercalation and adsorption,[83] this observation is likely a consequence of neglecting competition from Na$^+$ and K$^+$ transport. In electrodialysis, the bulk anion and cation ions are transported separately through the AEM and CEM, respectively, with Na$^+$, K$^+$, Li$^+$ and Mg^{2+} competing for cationic passage.[36] As a consequence of their similar charge density and higher diffusivity, Na$^+$ and K$^+$ are transported preferentially relative to Li$^+$, resulting in greater mobility coefficients within the CEM.[56] Coupled with electroneutrality constraints in the electrolyte streams,[11] the trans-CEM Li$^+$ flux decreases with salt-lake brines relative to binary cation solutions, attenuating the apparent Li$^+$/Mg^{2+} separation factors. The observed decline in Li$^+$/Mg^{2+} selectivity is amplified with Chinese salt-lake brines due to their greater Na$^+$/Li$^+$ ratio.[45]

In salt-lake lithium extraction, the hypersaline brine is typically acid pre-treated to a pH of 3 or lower, to mitigate scaling risks from carbonates and phosphates.[5,19,46] When contacted with acidified salt-lake brines, however, the CEM's monovalent selectivity exhibits a decreasing functional relationship with the solution pH; the measured $\alpha_{Li/Mg}$ values decline by 41.7 % when the pH is lowered from 7 to 3. Zeta potential experiments with pristine CEMs and AEMs, as depicted in Figure 3C, are used to evaluate the electric double layer characteristics,[51,52] with the measurements revealing a 37.9 % decrease in the interfacial potential of the diffuse layer, likely as a result of the weakening of the Donnan exclusion effect from the deprotonation of charged moieties of the surface layer under acidic conditions.[36,47] This coincides with an increase in the Mg^{2+} leakage by 18 % and a decrease in the Li$^+$, Na$^+$ and K$^+$ permeation by 14 % or greater, corroborating that Donnan exclusion weakening is the principal cause of the observed selectivity reduction.[39] Using the terminology defined in Figures 3D and E, the impact of the membrane charge density on Donnan partitioning is evaluated in Figure 3F and Supp. Figures 13A–C, for volumetric charge densities of 0.50, 1.68 and 5.0 M.[39,42] The molar ratio of Li$^+$/Mg^{2+} within the IEM decreases by an order of

magnitude as the charge density declines by 59.5 %, which corroborates the empirical inference of the weakening of Donnan exclusion under low solution pH.

The selectivity decline is further compounded under high feed salinities, with the experimental $\alpha_{Li/Mg}$ values for the Chilean and Chinese salt-lake brines attenuating from 5.85 and 4.10 at 10 g L^{-1} to 0.93 and 1.07 at 250 g L^{-1}, respectively. As illustrated in Fig. 3F, at a solution concentration of 10 g L^{-1} (0.35 M), a large molar partitioning ratio of 9.58 is obtained between the partitioned Li^+ and Mg^{2+}, as a result of Donnan exclusion. As monovalent ions, Donnan exclusion is ineffective in influencing the relative partitioning rates of Na^+ and K^+ relative to Li^+.[39] With the 250 g L^{-1} salt-lake brines, however, the molar ratio of Li^+/Mg^{2+} of the partitioned ions declines to 1.45 when the feed molarity exceeds the CEM's charge density, exemplifying the weakened efficacy of Donnan exclusion under hypersaline conditions.[39]

Further, upon prolonged exposure to salt-lake brine, degradation and delamination of the positive PEI coating has been reported by Ying et al.[49] The underlying negative PS-DVB substrate was exposed from the weakened interfacial adhesion energies and elevated osmosis-induced stresses.[49] Our zeta potential measurements (Fig. 3C) corroborate this observation, with the aged CEMs registering an average 24.7 mV decline and even switching signs at low pH. Compared to experiments with pristine IEMs, we consistently register attenuated Li^+/Mg^{2+} separation factors with aged IEMs, suggesting that irreversible damage of the PEI layer results from the salt-lake brine exposure, in agreement with recent reports.[78] In essence, our results underscore the detrimental impact from the high concentration and acidity of salt-lake brines on the efficacy of Donnan exclusion for Li^+ concentration, and accentuate the need to use representative multicomponent brines for selectivity characterization of novel IEMs.

3.3 Higher Current Densities Ameliorate Selectivity Degradation for Hypersaline Brines

In electrodialysis, for a given recovery ratio, higher current densities under 70 % of the limiting value are operationally favorable because it reduces the membrane area, system footprint and capital costs while improving the extraction kinetics.[34,36,84–86] Concurrently, higher current densities have been reported to improve co-ion/counter-ion selectivity in hypersaline applications with conventional
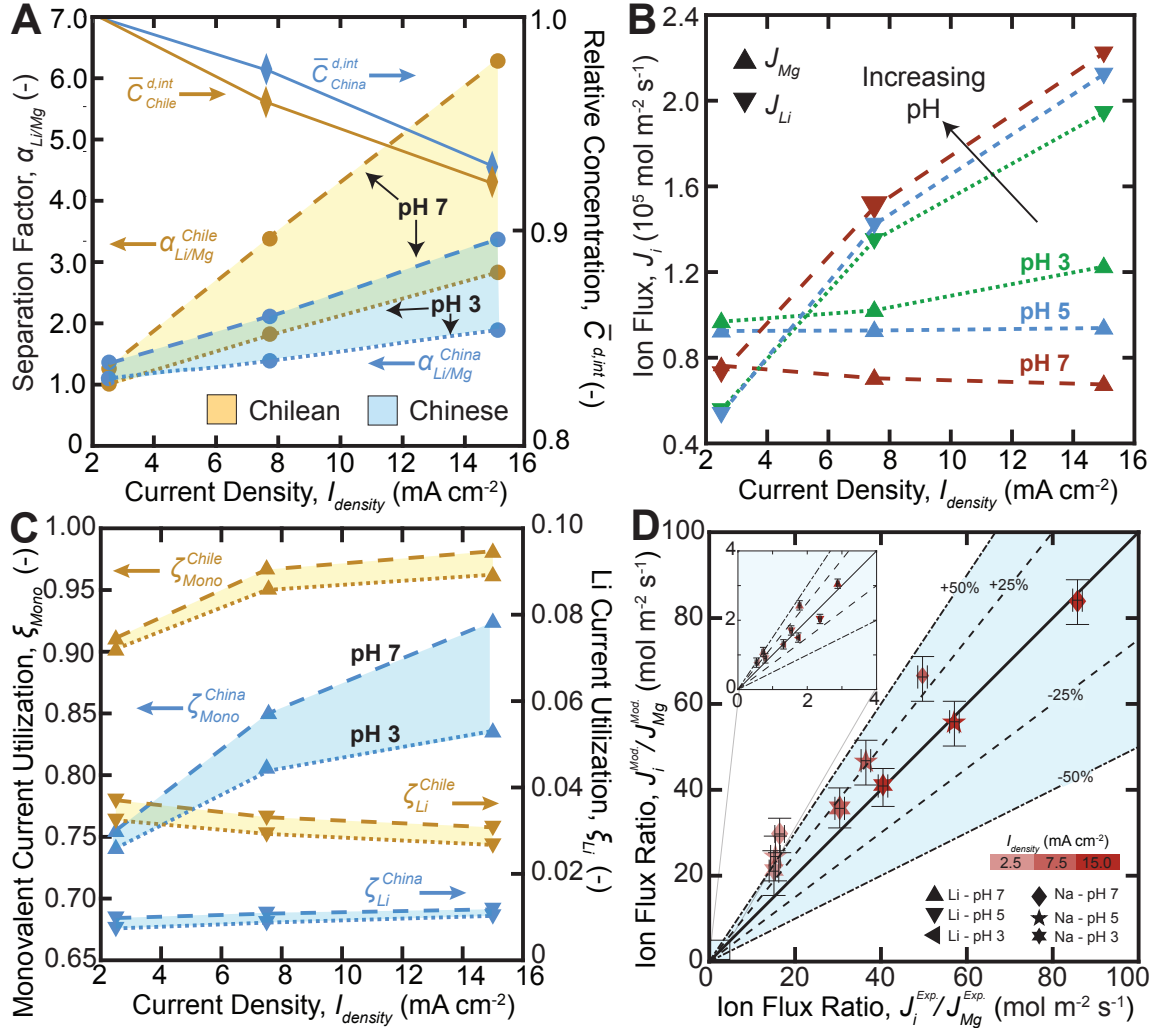
15

Figure 4: (**A**) Plot of the Li$^+$/Mg^{2+} separation factor (circles) and concentration polarization (diamonds) as a function of the applied current density for Chilean and Chinese brines, at solution concentration of 70 g L^{-1}, between the pH range from 3 to 7. The beige and blue colored bands represent the expected separation factors for the solution pH between 3 and 7, for the Chilean and Chinese salt-lake brines, respectively. Solutions with concentrations of 70 g L^{-1} in place of 250 g L^{-1} are used to investigate current density effects to circumvent practical limitations of bench-scale direct current power supply; (**B**) Impact of increasing current density on the ionic flux of Li$^+$ and Mg^{2+} for solution pH between 3 to 7. Mg^{2+} flux remains largely constant while the Li$^+$ flux increases almost linearly with current density. Greater increments in the Li$^+$/Mg^{2+} selectivity are recorded at pH 7 as a result of higher volumetric charge densities of the CEM; (**C**) The monovalent cation utilization increases while the Li$^+$ current utilization remains largely invariant with current density, indicating that the increased driving potentials promote the preferential permeation of Na$^+$ and K$^+$. (**D**) Plot of the ion flux ratios of the empirical measurements and model predictions, for Na$^+$ and Li$^+$ relative to Mg^{2+}, across the three tested current densities and solution pH. The diffusion coefficient uncertainties are estimated with Student's t-tests based on binary and ternary cation mixtures.[59] Na$^+$ diffusion coefficient uncertainties (± 33.1 %) are significantly higher than the corresponding values of Li$^+$ (± 8.7 %) owing to its higher concentration.

16

electrodialysis membranes.[36,81] The empirical Li^+/Mg^{2+} separation factors and the ion fluxes for the Chilean and Chinese salt-lake brines are presented in Figures 4A and B, between the current densities of 2.5 to 15.0 mA cm^{-2} and solution pH of 3 to 7. The derived $\alpha_{Li/Mg}$ values exhibit a near linear relationship ($\min_i r_i^2 \approx 0.975$) with the current density, increasing from 1.23 and 1.11 at 2.5 mA cm^{-2} to 6.25 and 3.37 at 15.0 mA cm^{-2} for the Chilean and Chinese compositions at pH 7, respectively. Comparatively, modest improvements in selectivity by a factor of 1.85 and 0.37 are recorded at pH 3 for the Chilean and Chinese brines. When the ion fluxes are deconvoluted at pH 7, we observe that Mg^{2+} flux remains largely invariant while the Li^+ flux increases monotonically when the current density is increased to 15.0 mA cm^{-2}. Over the same current density interval at pH 3, however, a 27.3 % increase in Mg^{2+} leakage is observed, which suggests that the selectivity enhancement from a higher current density is less effective with IEMs that have lower volumetric charge densities.

The influence of the applied current density on the monovalent cation (ξ_{Mono}) and Li^+ (ξ_{Li}) current utilizations is presented in Fig. 4C, with a larger Li^+ utilization factor indicating a more efficient use of electrical work for lithium extraction.[34,36] Experiments with Chilean salt-lake brines register monovalent cation current utilizations that are 9.1 to 20.2 % higher than the Chinese compositions, as a result of the lower Mg^{2+} concentrations in Chilean brines. When the current density is amplified to 15.0 mA cm^{-2}, we observe a 7.14 and 14.4 % increase in the average ξ_{Mono} values, for the Chilean and Chinese compositions, respectively. However, the current utilization by Li^+ decays by 10.6 % on average with the same current density increments, revealing that a less efficient electricity usage occurs at higher current densities from Na^+ and K^+ competition.

Counter-ion selectivity enhancements from higher current densities have been reported in the literature for a variety of resource recovery applications.[4,31,36,81,84,85] These enhancements have been qualitatively rationalized with mass transfer improvements from either: 1) the counter-ion conductivity; 2) the Donnan potential at equilibrium; or 3) the diluate stream concentration boundary layer. However, a formal mathematical treatment of the phenomena remains elusive. Here, a model based on the Nernst-Planck,[11] Donnan equilibrium[39,64] and extended Mackie-Meares[56] equations (Eq. 5) is employed to deconvolute the partitioning and mobility contributions, and the results are juxtaposed with the measurements in Figure 4D. The average absolute deviations for the Li^+/Mg^{2+} and Na^+/Mg^{2+} flux ratios are 19.0 and 29.7 %, respectively.

17

Our results suggest that the three phenomena are coupled and work synergistically to enhance the monovalent selectivity. As depicted in Figure 3E, in response to a higher current density, the interfacial ion concentration becomes further depleted, as a result of kinetic limitations arising from ion diffusion across the boundary layer in the bulk flow.[34,36] As a consequence, our model suggests that the dilutive effect along the membrane-solution interface enhances the counter-ion selectivity from Donnan exclusion, amplifying the resultant Donnan potential and the partition coefficients of monovalent cations. The selectivity enhancements from an improved Donnan exclusion of Mg^{2+} is amplified by the inherent higher mobility of monovalent cations within the CEM,[56] resulting in a greater than proportional increase in the apparent monovalent selectivity factors. The Li^+/Mg^{2+} and Na^+/Mg^{2+} flux ratios increase from 1.06 to 3.06 and from 29.8 to 83.8 at pH 7, respectively, when the partitioning factor (see Section A.2 in SI) is magnified from 2.60 to 7.65. This deduction aligns with the prior conclusions on counter-ion/co-ion selectivity mechanisms in ED.[81]

3.4 Trade-off between Selectivity and Energy Usage Intensifies in Salt-Lake Applications

Figure 5A illustrates the impact of feed concentration and solution pH on the Li^+/Mg^{2+} separation factor for the Chilean brine experiments with nanofiltration (NF) and electrodialysis. The NF separation factors are calculated with the asymptotic (maximum rejection) ion fluxes from prior salt-lake brine experiments with unmodified semi-aromatic polyamide NF membranes.[28] Similar to Fig. 3B, we observe decreased monovalent selectivity from the weakening of Donnan exclusion in high salinity brines at pH 2 in NF.[28] In contrast to ED, however, higher driving pressures in NF weaken Donnan exclusion by raising the interfacial concentrations, as a result of the intensified concentration boundary layers.[87] Our experiments demonstrate that a higher driving current density in ED sustains a favorable monovalent selectivity even in hypersaline conditions, illustrating an inherent advantage for salt-lake applications.

The current density impact on the Li^+ specific energy consumption and the thermodynamic (Second Law) efficiency is summarized in Figure 5B, for experiments with binary cation and multi-component salt-lake solutions. The SEC_{Li} is normalized to the corresponding values obtained with binary cation solutions. Our results show that the gains in monovalent selectivity at a higher cur-
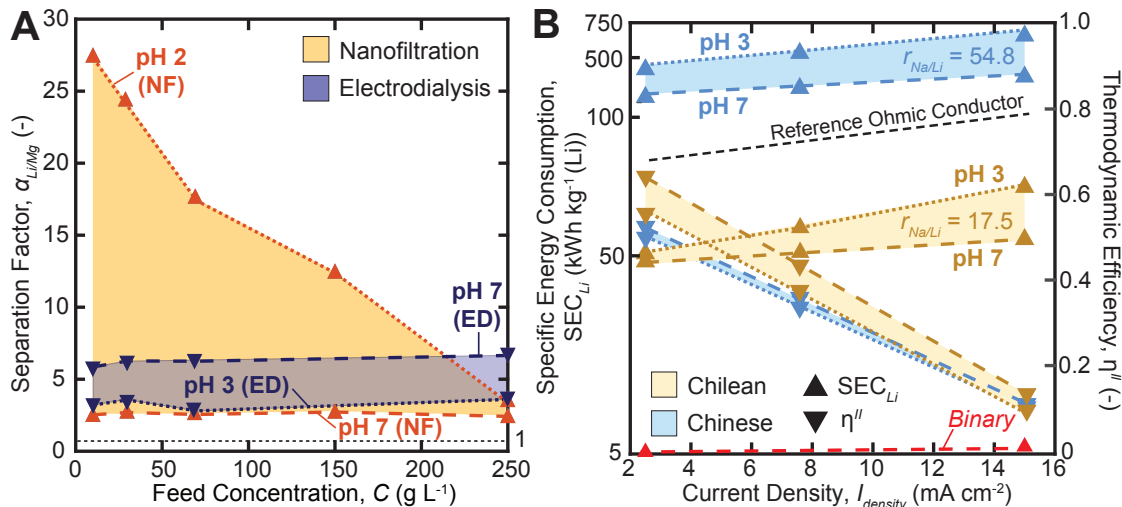
Figure 5: (**A**) Plot of the Li^+/Mg^{2+} separation factor as a function of the external bulk solution concentration for nanofiltration and electrodialysis, from experiments with brines based on Salar de Atacama, Chile. The NF separation factors are derived from the asymptotic (maximum) ion rejections for Li^+ and Mg^{2+} in our prior study.[28] The NF membrane from our prior study has an unmodified polyamide active layer, with an isoelectric point at pH 3.2 approximately. The unavoidable decline in Li^+/Mg^{2+} selectivity in NF under higher feed concentrations arises from weakening Donnan exclusion effects. On the other hand, with ED, high Li^+/Mg^{2+} selectivity can be maintained across the spectrum of feed concentrations, by raising the applied current density; (**B**) Plot of the specific energy consumption per mole of Li recovered and the thermodynamic (Second Law) efficiency as a function of the applied current density for Chilean and Chinese salt-lake brines. Higher current densities maintain high Li^+/Mg^{2+} selectivity under hypersaline feed concentrations, but they incur a significant increase in electrical work requirements, with more pronounced effects for Chinese salt-lake brines. The beige and blue colored bands represent the expected SEC_{Li} and η^{II} for the solution pH between 3 and 7, for the Chilean and Chinese salt-lake brines, respectively.

rent density are accompanied by a monotonic increase in the SEC_{Li}. For the Chilean and Chinese brines, the normalized SEC_{Li} increases by 71.6 and 45.5 % when the current density is increased from 2.5 to 15.0 mA cm^{-2}, respectively. The energy dissipated from joule heating in a constant impedance ohmic conductor exhibits a quadratic dependence on the current density.[34] Our SEC_{Li} measurements, however, reveal a power law exponent between 1.07 to 1.86, indicating that the effective impedance of the ED stack drops with increasing current densities. The higher resistance at pH 3 is caused by the poorer ionic conductivity of the IEM resulting from its lowered volumetric charge density, corroborating our prior conclusions on the weakened Donnan exclusion. Further, our measurements indicate that the normalized SEC_{Li} is largely linearly correlated with the solution's Na^+/Li^+ molar ratio. Consequently, our experiments reveal that SEC_{Li} projections based on binary cation solutions will underpredict the energy costs by a factor of 17.5 and 54.8 in Chilean

and Chinese salt-lakes, respectively.

When the current density increases from 2.5 to 15.0 mA cm^{-2}, a diminishing fraction of the input energy contributes to raising the chemical potentials of the product streams. Across the same current density interval, the optimal thermodynamic efficiency decreases from 62.5 to 8.42 % with Chilean brines, and from 46.9 to 9.20 % with Chinese brines. In essence, while the Li$^+$/Mg^{2+} selectivity can be enhanced by up to a factor of six with salt-lake brines, the higher current densities induce a greater than proportional increase in entropy generation and energy wastage by joule heating.[11] These results elucidated a steep trade-off between ion selectivity and energy efficiency in salt-lake lithium extraction that is governed by the applied current density.

4 Implications for Salt-Lake Lithium Concentration

We have elucidated the detrimental impacts of the high feed concentration and acidity of salt-lake brines on the selectivity mechanism and thermodynamic efficiency of electrodialysis, based on 1250 ion concentration measurements that span four salinities and three pH levels. With binary cation solutions, our experiments revealed that the Li$^+$/Mg^{2+} selectivity was overestimated by up to 250 % and the Li SEC was underpredicted by a factor of 54.8, as a consequence of neglecting Na$^+$ and K$^+$ competition. Further, our results demonstrated that the performance of electrodialysis is characterized by a steep trade-off between ion selectivity and energy efficiency at higher current densities: for hypersaline salt-lake brines, a 6.25 times enhancement in Li$^+$/Mg^{2+} selectivity was accompanied by a 71.6 % increase in the SEC, caused by unavoidable entropy generation that results from joule heating.

Here, we quantify the potential impact of our empirical findings on the process duration and land area requirements of salt-lake lithium concentration, using Salar de Atacama as a case study. The Salar de Atacama salt-lake concentrates 8.99 $\times 10^6$ moles of Li on average per day with 3000 km^2 of salt flat area.[1] Each production cycle takes approximately 2 years and consumes 2.7 $\times 10^6$ m^3 of fresh water, contributing to a price inelastic lithium supply that is slow to respond to market demand.[9,10] We leverage our experiments with 250 g L^{-1} Chilean brines to evaluate the energy and land area requirements in comparison to an industrial-scale ED module such as is typically employed in the salt production industry[11,33] (Section C.3 in SI). Here, the Chilean salt-lake brine

20

and a dilute NaCl (0.1 M) solution are used for the diluate and concentrate streams, respectively, to simulate DLE applications.[19] The land area impact of a photovoltaic solar farm is calculated, which incorporates the spatial demands from power generation, storage and transmission.[88]

Based on a 10 h daily production cycle, our results indicate that over 7.70×10^6 moles of Li can be extracted per day from the Chilean salt lake with a commercial-scale ED unit operation, using existing monovalent selective CEMs. The quantity of Li concentrated in a continuous ED module is nearly 85 % of the current production capacity of Salar de Atacama. Our results reveal that the Li^+/Mg^{2+} ratio increased from 0.57 in the feed stream to 4.01 in the product stream, suggesting that the resulting product is sufficiently pure for DLE.[17] Further, our model suggests that a photovoltaic farm with a total footprint between 11.35 to 12.84 km^2 operating for 10 h daily on existing salt flats can generate the required electrical work to sustain continuous Li concentration in the Chilean salt lake.[88] The normalized land requirement ($\overline{A}_{Li}$, Eq. 20 in SI) for ED is calculated to be between 1.21 to 1.67 m^2 mol^{-1}, which is less than 1 % of the corresponding value of 3.34×10^2 m^2 mol^{-1} obtained for the current evaporative practices in Chile. A full assessment of economic viability requires knowledge of Chilean interest and corporate tax rates, as well as permitting, labor and legal costs, which is difficult to ascertain accurately based on the existing information in published documents. Nevertheless, our technical findings suggest that an industrial-scale ED plant can replace evaporation ponds for lithium concentration while avoiding the negative environmental impacts of ponds.

Our results suggest that certain critical advancements in next-generation IEMs can unlock significant improvements in the techno-economic viability of DLE. To avoid the inherent selectivity-efficiency trade-off with salt-lakes ($\geq$ 4.0 M), the development of IEMs with volumetric charge densities of 5.0 M or greater in hypersaline conditions can potentially lower the land area impact by a factor of 3. With Na^+- and K^+–rejecting CEMs, the $\overline{A}_{Li}$ improves further by a factor of 21.2, indicating that the control of Na^+ and K^+ transport is the most sensitive variable for the optimization of lithium extraction from salt lakes.

Supporting Information Available

The following files are available in the Supporting Information.

21

- Original experimental data for 1250 electrodialysis ion concentration measurements with binary cation solutions and salt-lake brines.

- Model derivation and numerical algorithm to simulate ion and water transport in ion exchange membranes.

- Analysis of Donnan exclusion and case study assessment with Salar de Atacama.

Author Contributions

Z.H. Foo performed the experiments, programmed the numerical models, and conducted the technical analysis. J.B. Thomas, S.M. Heath and J.A. Garcia assisted with the experiments. J.H. Lienhard led the technical analysis and supervised the project. The manuscript was prepared and reviewed by all authors.

Declaration of Competing Interest

The authors declare no competing financial or personal conflicts of interest that could have appeared to influence the content of this paper.

Acknowledgements

22

References

(1) Vera, M. L.; Torres, W. R.; Galli, C. I.; Chagnes, A.; Flexer, V. Environmental impact of direct lithium extraction from brines. *Nature Reviews Earth & Environment* **2023**, *4*, 149–165.

(2) Xu, C.; Dai, Q.; Gaines, L.; Hu, M.; Tukker, A.; Steubing, B. Future material demand for automotive lithium-based batteries. *Communications Materials* **2020**, *1*, 99.

(3) Kumar, A.; Fukuda, H.; Hatton, T. A.; Lienhard, J. H. Lithium Recovery from Oil and Gas Produced Water: A Need for a Growing Energy Industry. *ACS Energy Letters* **2019**, *4*, 1471–1474.

(4) Ying, J.; Lin, Y.; Zhang, Y.; Yu, J. Developmental Progress of Electrodialysis Technologies and Membrane Materials for Extraction of Lithium from Salt Lake Brines. *ACS ES&T Water* **2023**, *3*, 1720–1739.

(5) Khalil, A.; Mohammed, S.; Hashaikeh, R.; Hilal, N. Lithium recovery from brine: Recent developments and challenges. *Desalination* **2022**, *528*, 115611.

(6) Alam, M. A.; Sepúlveda, R. Environmental degradation through mining for energy resources: The case of the shrinking Laguna Santa Rosa wetland in the Atacama Region of Chile. *Energy Geoscience* **2021**, *3*, 182–190.

(7) Liu, W.; Agusdinata, D. B. Interdependencies of lithium mining and communities sustainability in Salar de Atacama, Chile. *Journal of Cleaner Production* **2020**, *260*, 120838.

(8) Huang, T.-Y.; Pérez-Cardona, R.; Zhao, F.; Sutherland, J. W.; Parans Paranthaman, M. Life Cycle Assessment and Techno-Economic Assessment of Lithium Recovery from Geothermal Brine. *ACS Sustainable Chemistry & Engineering* **2021**, *9*, 6551–6560.

(9) Xu, P.; Hong, J.; Qian, X.; Xu, Z.; Xia, H.; Tao, X.; Xu, Z.; Ni, Q. Q. Materials for lithium recovery from salt lake brine. *Journal of Materials Science* **2021**, *56*, 16–63.

(10) Olivetti, E. A.; Ceder, G.; Gaustad, G. G.; Fu, X. Lithium-Ion Battery Supply Chain Considerations: Analysis of Potential Bottlenecks in Critical Metals. *Joule* **2017**, *1*, 229–243.

(11) McGovern, R. K.; Weiner, A. M.; Sun, L.; Chambers, C. G.; Zubair, S. M.; Lienhard, J. H. On the cost of electrodialysis for the desalination of high salinity feeds. *Applied Energy* **2014**, *136*, 649–661.

(12) Su, H.; Li, Z.; Zhang, J.; Liu, W.; Zhu, Z.; Wang, L.; Qi, T. Combining Selective Extraction and Easy Stripping of Lithium Using a Ternary Synergistic Solvent Extraction System through Regulation of Fe3+ Coordination. *ACS Sustainable Chemistry and Engineering* **2020**, *8*, 1971–1979.

(13) Yuan, Z.; Liu, H.; Yong, W. F.; She, Q.; Esteban, J. Status and advances of deep eutectic solvents for metal separation and recovery. *Green Chemistry* **2022**, *24*, 1895–1929.

(14) Hanada, T.; Goto, M. Synergistic Deep Eutectic Solvents for Lithium Extraction. *ACS Sustainable Chemistry & Engineering* **2021**, *9*, 2152–2160.

(15) McNally, J. S.; Foo, Z. H.; Deshmukh, A.; Orme, C. J.; Lienhard, J. H.; Wilson, A. D. Solute displacement in the aqueous phase of water-NaCl-organic ternary mixtures relevant to solvent-driven water treatment. *RSC Advances* **2020**, *10*, 29516–29527.

(16) Foo, Z. H.; Stetson, C.; Dach, E.; Deshmukh, A.; Lee, H.; Menon, A. K.; Prasher, R.; Yip, N. Y.; Lienhard, J. H.; Wilson, A. D. Solvent-driven aqueous separations for hypersaline brine concentration and resource recovery. *Trends in Chemistry* **2022**, *4*, 1078–1093.

(17) Battaglia, G.; Berkemeyer, L.; Cipollina, A.; Cortina, J. L.; Fernandez De Labastida, M.; Lopez Rodriguez, J.; Winter, D. Recovery of Lithium Carbonate from Dilute Li-Rich Brine via Homogenous and Heterogeneous Precipitation. *Industrial & Engineering Chemistry Research* **2022**, *2022*, 13589–13602.

(18) Deshmukh, A.; Foo, Z. H.; Stetson, C.; Lee, H.; Orme, C. J.; Wilson, A. D.; Lienhard, J. H. Thermodynamics of solvent-driven water extraction from hypersaline brines using dimethyl ether. *Chemical Engineering Journal* **2022**, *434*, 134391.

(19) Alkhadra, M. A.; Su, X.; Suss, M. E.; Tian, H.; Guyes, E. N.; Shocron, A. N.; Conforti, K. M.; Pedro De Souza, J.; Kim, N.; Tedesco, M.; Khoiruddin, K.; Wenten, G.; Santiago, J. G.;

Hatton, T. A.; Bazant, M. Z. Electrochemical Methods for Water Purification, Ion Separations, and Energy Conversion. *Chemical Reviews* **2022**, *122*, 13547–13635.

(20) Yang, L.; Gao, Z.; Liu, T.; Huang, M.; Liu, G.; Feng, Y.; Shao, P.; Luo, X. Direct Electrochemical Leaching Method for High-Purity Lithium Recovery from Spent Lithium Batteries. *Environmental Science & Technology* **2023**, *57*, 4591–4597.

(21) Wang, H.; Jones, L. O.; Hwang, I.; Allen, M. J.; Tao, D.; Lynch, V. M.; Freeman, B. D.; Khashab, N. M.; Schatz, G. C.; Page, Z. A.; Sessler, J. L. Selective Separation of Lithium Chloride by Organogels Containing Strapped Calix[4]pyrroles. *Journal of the American Chemical Society* **2021**, *143*, 20403–20410.

(22) Sachar, H. S.; Zofchak, E. S.; Marioni, N.; Zhang, Z.; Kadulkar, S.; Duncan, T. J.; Freeman, B. D.; Ganesan, V. Impact of Cation-Ligand Interactions on the Permselectivity of Ligand-Functionalized Polymer Membranes in Single and Mixed Salt Systems. *Macromolecules* **2022**, *55*, 4821–4831.

(23) Murphy, O.; Haji, M. N. A review of technologies for direct lithium extraction from low Li+ concentration aqueous solutions. *Frontiers in Chemical Engineering* **2022**, *4*, 112.

(24) Wu, L.; Zhang, C.; Kim, S.; Hatton, T. A.; Mo, H.; David Waite, T. Lithium recovery using electrochemical technologies: Advances and challenges. *Water Research* **2022**, *221*, 118822.

(25) Li, H.; Wang, Y.; Li, T.; Ren, X.-k.; Wang, J.; Wang, Z.; Zhao, S. Nanofiltration Membrane with Crown Ether as Exclusive Li+ Transport Channels Achieving Efficient Extraction of Lithium from Salt Lake Brine. *Chemical Engineering Journal* **2022**, *438*, 135658.

(26) Wang, R.; He, R.; He, T.; Elimelech, M.; Lin, S. Performance metrics for nanofiltration-based selective separation for resource extraction and recovery. *Nature Water* **2023**, *1*, 291–300.

(27) Guo, C.; Qian, Y.; Liu, P.; Zhang, Q.; Zeng, X.; Xu, Z.; Zhang, S.; Li, N.; Qian, X.; Yu, F. One-Step Construction of the Positively/Negatively Charged Ultrathin Janus Nanofiltration Membrane for the Separation of Li + and Mg 2+. *ACS Applied Materials & Interfaces* **2023**, *15*, 4814–4825.

(28) Foo, Z. H.; Rehman, D.; Bouma, A. T.; Monsalvo, S.; Lienhard, J. H. Lithium Concentration from Salt-Lake Brine by Donnan-Enhanced Nanofiltration. *Environmental Science & Technology* **2023**, *57*, 6320–6330.

(29) Shi, M.; Diaz, L. A.; Klaehn, J. R.; Wilson, A. D.; Lister, T. E. Li2CO3 Recovery through a Carbon-Negative Electrodialysis of Lithium-Ion Battery Leachates. *ACS Sustainable Chemistry & Engineering* **2022**, *10*, 11773–11781.

(30) Qiu, Y.; Ruan, H.; Tang, C.; Yao, L.; Shen, J.; Sotto, A. Study on recovering high-concentration lithium salt from lithium-containing wastewater using a hybrid reverse osmosis (RO)-electrodialysis (ED) process. *ACS Sustainable Chemistry & Engineering* **2019**, *7*, 13481–13490.

(31) Chen, Q. B.; Ji, Z. Y.; Liu, J.; Zhao, Y. Y.; Wang, S. Z.; Yuan, J. S. Development of recovering lithium from brines by selective-electrodialysis: Effect of coexisting cations on the migration of lithium. *Journal of Membrane Science* **2018**, *548*, 408–420.

(32) White, N.; Misovich, M.; Alemayehu, E.; Yaroshchuk, A.; Bruening, M. L. Highly selective separations of multivalent and monovalent cations in electrodialysis through Nafion membranes coated with polyelectrolyte multilayers. *Polymer* **2015**, *103*, 478–485.

(33) Nayar, K. G.; Fernandes, J.; McGovern, R. K.; Al-Anzi, B. S.; Lienhard, J. H. Cost and energy needs of RO-ED-crystallizer systems for zero brine discharge seawater desalination. *Desalination* **2019**, 115–132.

(34) Strathmann, H. *Ion-exchange membrane separation processes*; Elsevier, 2004.

(35) Ahdab, Y. D.; Rehman, D.; Schücking, G.; Barbosa, M.; Lienhard, J. H. Treating Irrigation Water Using High-Performance Membranes for Monovalent Selective Electrodialysis. *ACS ES&T Water* **2021**, *1*, 117–124.

(36) Luo, T.; Abdu, S.; Wessling, M. Selectivity of ion exchange membranes: A review. *Journal of Membrane Science* **2018**, *555*, 429–454.

(37) Kingsbury, R. S.; Zhu, S.; Flotron, S.; Coronell, O. Microstructure Determines Water and Salt Permeation in Commercial Ion-Exchange Membranes. *ACS Applied Materials & Interfaces* **2018**, *10*, 39745–39756.

(38) Wang, L.; Cao, T.; Pataroque, K. E.; Kaneda, M.; Maarten Biesheuvel, P.; Elimelech, M. Significance of Co-ion Partitioning in Salt Transport through Polyamide Reverse Osmosis Membranes. *Environmental Science & Technology* **2023**, *57*, 3930–3939.

(39) Fan, H.; Yip, N. Y. Elucidating conductivity-permselectivity tradeoffs in electrodialysis and reverse electrodialysis by structure-property analysis of ion-exchange membranes. *Journal of Membrane Science* **2019**, *573*, 668–681.

(40) Yip, N. Y.; Elimelech, M. Comparison of energy efficiency and power density in pressure retarded osmosis and reverse electrodialysis. *Environmental Science & Technology* **2014**, *48*, 11002–11012.

(41) Aydogan Gokturk, P.; Sujanani, R.; Qian, J.; Wang, Y.; Katz, L. E.; Freeman, B. D.; Crumlin, E. J. The Donnan potential revealed. *Nature Communications* **2022**, *13*, 1–7.

(42) Ding, D.; Yaroshchuk, A.; Bruening, M. L. Electrodialysis through nafion membranes coated with polyelectrolyte multilayers yields >99% pure monovalent ions at high recoveries. *Journal of Membrane Science* **2022**, *647*, 120294.

(43) Duchanois, R. M.; Mazurowski, L.; Fan, H.; Verduzco, R.; Nir, O.; Elimelech, M. Precise Cation Separations with Composite Cation-Exchange Membranes: Role of Base Layer Properties. *Environmental Science and Technology* **2023**, *57*, 6331–6341.

(44) Nie, X. Y.; Sun, S. Y.; Sun, Z.; Song, X.; Yu, J. G. Ion-fractionation of lithium ions from magnesium ions by electrodialysis using monovalent selective ion-exchange membranes. *Desalination* **2017**, *403*, 128–135.

(45) Xu, S.; Song, J.; Bi, Q.; Chen, Q.; Zhang, W. M.; Qian, Z.; Zhang, L.; Xu, S.; Tang, N.; He, T. Extraction of lithium from Chinese salt-lake brines by membranes: Design and practice. *Journal of Membrane Science* **2021**, *635*, 376–7388.

(46) Meshram, P.; Pandey, B. D.; Mankhand, T. R. Extraction of lithium from primary and secondary sources by pre-treatment, leaching and separation: A comprehensive review. *Hydrometallurgy* **2014**, *150*, 192–208.

(47) Ritt, C. L.; Werber, J. R.; Wang, M.; Yang, Z.; Zhao, Y.; Kulik, H. J.; Elimelech, M. Ionization behavior of nanoporous polyamide membranes. *Proceedings of the National Academy of Sciences of the United States of America* **2020**, *117*, 30191–30200.

(48) Park, S. H.; Kim, J. H.; Moon, S. J.; Jung, J. T.; Wang, H. H.; Ali, A.; Quist-Jensen, C. A.; Macedonio, F.; Drioli, E.; Lee, Y. M. Lithium recovery from artificial brine using energy-efficient membrane distillation and nanofiltration. *Journal of Membrane Science* **2020**, *598*, 117683.

(49) Ying, J.; Lin, Y.; Zhang, Y.; Jin, Y.; Li, X.; She, Q.; Matsuyama, H.; Yu, J. Mechanistic insights into the degradation of monovalent selective ion exchange membrane towards long-term application of real salt lake brines. *Journal of Membrane Science* **2022**, *652*, 120446.

(50) Liu, H.; Ruan, H.; Zhao, Y.; Pan, J.; Sotto, A.; Gao, C.; Van Der Bruggen, B.; Shen, J. A facile avenue to modify polyelectrolyte multilayers on anion exchange membranes to enhance monovalent selectivity and durability simultaneously. *Journal of Membrane Science* **2017**, *543*, 310–318.

(51) Elimelech, M.; Chen, W. H.; Waypa, J. J. Measuring the zeta (electrokinetic) potential of reverse osmosis membranes by a streaming potential analyzer. *Desalination* **1994**, *95*, 269–286.

(52) Xie, H.; Saito, T.; Hickner, M. A. Zeta potential of ion-conductive membranes by streaming current measurements. *Langmuir* **2011**, *27*, 4721–4727.

(53) Rehman, D.; Ahdab, Y. D.; Lienhard, J. H. Monovalent selective electrodialysis: Modelling multi-ionic transport across selective membranes. *Water Research* **2021**, *199*, 117171.

(54) Mubita, T. M.; Porada, S.; Biesheuvel, P. M.; van der Wal, A.; Dykstra, J. E. Strategies to increase ion selectivity in electrodialysis. *Separation and Purification Technology* **2022**, *292*, 120944.

(55) Fidaleo, M.; Moresi, M. Optimal strategy to model the electrodialytic recovery of a strong electrolyte. *Journal of Membrane Science* **2005**, *260*, 90–111.

(56) Fan, H.; Huang, Y.; Billinge, I. H.; Bannon, S. M.; Geise, G. M.; Yip, N. Y. Counterion Mobility in Ion-Exchange Membranes: Spatial Effect and Valency-Dependent Electrostatic Interaction. *ACS ES&T Engineering* **2022**, *2*, 1274–1286.

(57) Foo, Z. H.; Rehman, D.; Coombs, O. Z.; Deshmukh, A.; Lienhard, J. H. Multicomponent Fickian solution-diffusion model for osmotic transport through membranes. *Journal of Membrane Science* **2021**, *640*, 119819.

(58) Ahdab, Y. D.; Rehman, D.; Lienhard, J. H. Brackish water desalination for greenhouses: Improving groundwater quality for irrigation using monovalent selective electrodialysis reversal. *Journal of Membrane Science* **2020**, *610*, 118072.

(59) Wambui Mutoru, J.; Firoozabadi, A. Form of multicomponent Fickian diffusion coefficients matrix. *Journal of Chemical Thermodynamics* **2011**, *43*, 1192–1203.

(60) Laliberté, M.; Cooper, W. E. Model for calculating the density of aqueous electrolyte solutinos. *Journal of Chemical and Engineering Data* **2004**, *49*, 1141–1151.

(61) Laliberté, M. Model for calculating the viscosity of aqueous solutions. *Journal of Chemical and Engineering Data* **2007**, *52*, 321–335.

(62) Alkhadra, M. A.; Conforti, K. M.; Gao, T.; Tian, H.; Bazant, M. Z. Continuous Separation of Radionuclides from Contaminated Water by Shock Electrodialysis. *Environmental Science & Technology* **2019**, *54*, 527–536.

(63) Kamcev, J.; Paul, D. R.; Freeman, B. D. Ion activity coefficients in ion exchange polymers: Applicability of Manning's counterion condensation theory. *Macromolecules* **2015**, *48*, 8011–8024.

(64) Kamcev, J.; Galizia, M.; Benedetti, F. M.; Jang, E.-S.; Paul, D. R.; Freeman, B. D.; Manning, G. S. Partitioning of mobile ions between ion exchange polymers and aqueous salt solu-

tions: importance of counter-ion condensation †. *Physical Chemistry Chemical Physics* **2016**, *18*, 6021.

(65) Kitto, D.; Kamcev, J. Manning condensation in ion exchange membranes: A review on ion partitioning and diffusion models. *Journal of Polymer Science* **2022**, *60*, 2929–2973.

(66) Kim, H. T.; Frederick, W. J. Evaluation of Pitzer Ion Interaction Parameters of Aqueous Electrolytes at 25°C. 1. Single Salt Parameters. *Journal of Chemical and Engineering Data* **1988**, *33*, 177–184.

(67) Kim, H. T.; Frederick, W. J. Evaluation of pitzer ion interaction parameters of aqueous mixed electrolyte solutions at 25 °C. 2. Ternary mixing parameters. *Journal of Chemical and Engineering Data* **1988**, *33*, 278–283.

(68) Kingsbury, R. S.; Wang, J.; Coronell, O. Comparison of water and salt transport properties of ion exchange, reverse osmosis, and nanofiltration membranes for desalination and energy applications. *Journal of Membrane Science* **2020**, *604*, 117998.

(69) Liu, H.; She, Q. Influence of membrane structure-dependent water transport on conductivity-permselectivity trade-off and salt/water selectivity in electrodialysis: Implications for osmotic electrodialysis using porous ion exchange membranes. *Journal of Membrane Science* **2022**, *650*, 120398.

(70) Virtanen, P.; Gommers, R.; Oliphant, T. E.; Haberland, M.; Reddy, T.; Cournapeau, D.; Burovski, E.; Peterson, P.; Weckesser, W.; Bright, J.; van der Walt, S. J.; Brett, M.; Wilson, J.; Millman, K. J.; Mayorov, N.; Nelson, A. R.; Jones, E.; Kern, R.; Larson, E.; Carey, C. J.; Polat, ; Feng, Y.; Moore, E. W.; VanderPlas, J.; Laxalde, D.; Perktold, J.; Cimrman, R.; Henriksen, I.; Quintero, E. A.; Harris, C. R.; Archibald, A. M.; Ribeiro, A. H.; Pedregosa, F.; van Mulbregt, P.; Vijaykumar, A.; Bardelli, A. P.; Rothberg, A.; Hilboll, A.; Kloeckner, A.; Scopatz, A.; Lee, A.; Rokem, A.; Woods, C. N.; Fulton, C.; Masson, C.; Häggström, C.; Fitzgerald, C.; Nicholson, D. A.; Hagen, D. R.; Pasechnik, D. V.; Olivetti, E.; Martin, E.; Wieser, E.; Silva, F.; Lenders, F.; Wilhelm, F.; Young, G.; Price, G. A.; Ingold, G. L.; Allen, G. E.; Lee, G. R.; Audren, H.; Probst, I.; Dietrich, J. P.; Silterra, J.; Webber, J. T.;

30

Slavič, J.; Nothman, J.; Buchner, J.; Kulick, J.; Schönberger, J. L.; de Miranda Cardoso, J. V.; Reimer, J.; Harrington, J.; Rodríguez, J. L. C.; Nunez-Iglesias, J.; Kuczynski, J.; Tritz, K.; Thoma, M.; Newville, M.; Kümmerer, M.; Bolingbroke, M.; Tartre, M.; Pak, M.; Smith, N. J.; Nowaczyk, N.; Shebanov, N.; Pavlyk, O.; Brodtkorb, P. A.; Lee, P.; McGibbon, R. T.; Feldbauer, R.; Lewis, S.; Tygier, S.; Sievert, S.; Vigna, S.; Peterson, S.; More, S.; Pudlik, T.; Oshima, T.; Pingel, T. J.; Robitaille, T. P.; Spura, T.; Jones, T. R.; Cera, T.; Leslie, T.; Zito, T.; Krauss, T.; Upadhyay, U.; Halchenko, Y. O.; Vázquez-Baeza, Y. SciPy 1.0: fundamental algorithms for scientific computing in Python. *Nature Methods* **2020**, *17*, 261–272.

(71) Wang, R.; Zhang, J.; Tang, C. Y.; Lin, S. Understanding Selectivity in Solute-Solute Separation: Definitions, Measurements, and Comparability. *Environmental Science & Technology* **2022**, *56*, 2605–2616.

(72) Li, Y.; Wang, R.; Shi, S.; Cao, H.; Yin Yip, N.; Lin, S. Bipolar Membrane Electrodialysis for Ammonia Recovery from Synthetic Urine: Experiments, Modeling, and Performance Analysis. *Environmental Science & Technology* **2021**, *55*, 14886–14896.

(73) Mistry, K. H.; Lienhard, J. H. Generalized least energy of separation for desalination and other chemical separation processes. *Entropy* **2013**, *15*, 2046–2080.

(74) Martí-Calatayud, M. C.; Buzzi, D. C.; García-Gabaldón, M.; Bernardes, A. M.; Tenório, J. A.; Pérez-Herranz, V. Ion transport through homogeneous and heterogeneous ion-exchange membranes in single salt and multicomponent electrolyte solutions. *Journal of Membrane Science* **2014**, *466*, 45–57.

(75) Długołecki, P.; Anet, B.; Metz, S. J.; Nijmeijer, K.; Wessling, M. Transport limitations in ion exchange membranes at low salt concentrations. *Journal of Membrane Science* **2010**, *346*, 163–171.

(76) Epsztein, R.; Shaulsky, E.; Qin, M.; Elimelech, M. Activation behavior for ion permeation in ion-exchange membranes: Role of ion dehydration in selective transport. *Journal of Membrane Science* **2019**, *580*, 316–326.

(77) Shefer, I.; Lopez, K.; Straub, A. P.; Epsztein, R. Applying Transition-State Theory to Explore Transport and Selectivity in Salt-Rejecting Membranes: A Critical Review. *Environmental Science & Technology* **2022**, *14*, 11.

(78) Ahdab, Y. D.; Schücking, G.; Rehman, D.; Lienhard, J. H. Cost effectiveness of conventionally and solar powered monovalent selective electrodialysis for seawater desalination in greenhouses. *Applied Energy* **2021**, *301*, 117425.

(79) Stolov, M.; Freger, V. Membrane Charge Weakly Affects Ion Transport in Reverse Osmosis. *Environmental Science & Technology Letters* **2020**, *7*, 440–445.

(80) Zhang, L.; Biesheuvel, P. M.; Ryzhkov, I. I. Theory of Ion and Water Transport in Electron-Conducting Membrane Pores with p H-Dependent Chemical Charge. *Physical Review Applied* **2019**, *12*, 014039.

(81) Abu-Rjal, R.; Chinaryan, V.; Bazant, M. Z.; Rubinstein, I.; Zaltzman, B. Effect of concentration polarization on permselectivity. *Physical Review E* **2014**, *89*, 012302.

(82) Guo, C.; Li, N.; Qian, X.; Shi, J.; Jing, M.; Teng, K.; Xu, Z. Ultra-thin double Janus nanofiltration membrane for separation of Li + and Mg 2+ : "Drag" effect from carboxyl-containing negative interlayer-thin Double Janus NF membrane Hydrophobic/hydrophilic Positive/negative charge Separation of Li + and Mg 2+. *Separation and Purification Technology* **2020**, *230*, 115567.

(83) Yan, G.; Wang, M.; Hill, G. T.; Zou, S.; Liu, C. Defining the challenges of Li extraction with olivine host: The roles of competitor and spectator ions. *Proceedings of the National Academy of Sciences of the United States of America* **2022**, *119*, e2200751119.

(84) Dong, T.; Yao, J.; Wang, Y.; Luo, T.; Han, L. On the permselectivity of di-and mono-valent cations: Influence of applied current density and ionic species concentration. *Desalination* **2020**, *488*, 114521.

(85) Yang, D.; Liu, H.; She, Q. Mixed cation transport behaviours in electrodialysis during simultaneous ammonium enrichment and wastewater desalination. *Desalination* **2023**, *545*.

(86) Wu, L.; Luo, T.; Yang, X.; Zhao, H.; Wang, X.; Zhang, Z. Impact of the Donnan electrolytes on selectivity of cation exchange membranes evaluated via the ionic membrane conductivity. *Separation and Purification Technology* **2023**, *316*, 1383–5866.

(87) Wang, R.; Lin, S. Pore model for nanofiltration: History, theoretical framework, key predictions, limitations, and prospects. *Journal of Membrane Science* **2021**, *620*.

(88) Palmer-Wilson, K.; Donald, J.; Robertson, B.; Lyseng, B.; Keller, V.; Fowler, M.; Wade, C.; Scholtysik, S.; Wild, P.; Rowe, A. Impact of land requirements on electricity system decarbonisation pathways. *Energy Policy* **2019**, *129*, 193–205.

720 # TOC Graphic

721